Evaluation of Comparative Cytochrome P450 2B4 Model by Photoaffinity Labeling

P. Hodek[1], B. Sopko[1], L. Antonovič[2], M. Šulc[1,3], P. Novák[3] and H. W. Strobel[2]

[1] *Charles University, Department of Biochemistry, Hlavova 2030, 128 40 Praha 2, Czech Republic*
[2] *University of Texas Medical School at Houston, Department of Biochemistry and Molecular Biology, P.O.Box 20708, Texas 77225, U.S.A.*
[3] *Institute of Microbiology, Academy of Sciences of the Czech Republic, Vídeňská 1083, 142 20 Praha 4, Czech Republic*

Abstract. A homology model of rabbit CYP 2B4 was constructed on the basis of the crystallographic structure of truncated mammalian CYP 2C5/3 and bacterial soluble CYPs. To validate the CYP 2B4 homology model photoaffinity labeling was employed. Three probes (I–III) containing a photo-labile azido-group and an amino-group on opposite ends of the molecule were designed for photoaffinity labeling of the CYP 2B4 in increasing distance from the heme iron. Spectroscopic data proved probes I (the shortest) and II (a middle sized) to be coordinated with the heme iron *via* their amino-groups in the enzyme active center while the probe III (the longest) was not bound in this way. This binding orientation of probes I and II is in accordance with the model predicting ion-pairing of the negatively charged side chain of CYP 2B4 Asp 105 and a positively charged nitrogen located in an appropriate position in structures of probes I and II, only. The lack of heme binding of the probe III is clear from its docking into the CYP 2B4 model since no Asp 105 ion-pairing is possible. The target of photoactivated probe II, Arg 197, in a distance of about 16.5 Å from the heme iron, exactly matches the position of that amino acid residue, predicted from the CYP 2B4 homology model. Moreover, using this technique, a substrate access channel has been identified. To assess the predicted substrate-binding pocket, an interaction of a specific CYP 2B4 substrate, diamantane, was examined. In "silico" docking revealed strong binding of diamantane in an orientation allowing experimentally observed C4-hydroxylation. Our homology model of CYP 2B4 is thus consistent with experimental metabolic and photoaffinity labeling data.

Correspondence to: Petr Hodek, Charles University, Department of Biochemistry, Hlavova 2030, 128 40 Praha 2, Czech Republic. E-mail: hodek@natur.cuni.cz

Key words: CYP 2B4 — Comparative modeling — Photoaffinity probes — Active center

Abbreviations: CYP, cytochrome P450; PB, phenobarbital; Ms, liver microsomes; 3D, three-dimensional; PSD, post source decay; K_s, spectral dissociation constant; PDB, protein data bank; MALDI-TOF, matrix-assisted laser desorption ionization – time of flight; TFA, trifluoroacetic acid; BCA, bicinchoninic acid; Lys-C, endoproteinase cleaving peptide bonds C-terminally at lysine.

Introduction

The key enzyme of the mixed-function oxidase system, cytochrome P450 (EC 1.14.14.1), plays a major role in the biotransformation of many drugs, environmental pollutants, steroids, fatty acids, bile acids, and, frequently, also in activation of carcinogens (Porter and Coon 1991). Cytochromes P450 (CYPs) are a superfamily of hemoprotein enzymes which differ in their substrate specificity and are regulated by numerous factors including age, sex, and exposure to certain CYP inducers. Because of CYP general importance in both drug metabolism and carcinogen activation, elucidation of key structural elements for substrate recognition (leading to their metabolic oxidation) is of considerable interest. However, our understanding of this process has been limited by the lack of three-dimensional (3D) structures for mammalian CYPs. An increasing number of 3D structures of soluble microbial CYP determined by X-ray crystallography is becoming available: CYP 101 (Poulos et al. 1985), CYP 102 (Ravichandran et al. 1993), CYP 105 (Ito et al. 1999), CYP 107A1 (Cupp-Vickery and Poulos 1995), CYP 108 (Hasemann et al. 1994), CYP 119 (Yano et al. 2000), CYP 121 (Park et al. 1997), CYP 154C1 (Podust et al. 2003), CYP 165B3 (Zerbe et al. 2002), CYP 51 (Podust et al. 2001), CYP 55A1 (Leys et al. 2003). Since mammalian CYPs are integral membrane proteins, their crystallization is difficult. Only recently, crystallization and X-ray data of solubilized (truncated) mammalian CYP 2C5/3, CYP 2C9 and CYP 2B4 were published (Williams et al. 2000a, 2003; Scott et al. 2003) and the structural data deposited in the protein data bank (PDB). Mammalian CYPs have to be significantly changed (elimination of N-terminal transmembrane domain, modification of N-terminus and addition of C-terminal 4 × His tag) to be suitable for expression in bacteria, purification and crystal generation. The process of crystallization might be associated with further structural perturbations originating from e.g. CYP dimerization. This is possibly the case of the reported crystal structure of CYP 2B4 (Scott et al. 2003) showing an unusually large open cleft through which both monomers are interconnected to form a homodimer. It is not known whether the wild type of CYP 2B4, when exposed to its natural membrane/water environment, is also able to adopt the conformation seen in the crystal of truncated CYP 2B4.

Beside the X-ray crystallography, method of homology (comparative) modeling is an alternative technique employed for protein structural studies. Since there are significant similarities of overall structures of bacterial and mammalian CYPs, one

may presume conserved "protein fold" common to all CYPs (Nelson and Strobel 1988). Thus, 3D models of mammalian CYPs, based on expected global structure homology among CYPs, have been constructed using templates of known CYPs structures (Ekins et al. 2001; Lewis 2002). In this paper, we focus on the construction of a homology model of CYP 2B4 and its evaluation. CYP 2B4 shows 50.7% sequence identity with the template CYP 2C5/3 molecule, that is 2.5–3 times higher identity than with microbial CYPs. Therefore, the homology model based on the crystal structure of CYP 2C5/3 is expected to provide a significant improvement compared to former models based on the microbial CYPs. Homology models allow us to gain the insight into the relationship between CYP structure and its function, providing a base for the rational drug design and prediction of potential drug-drug interactions. It may also help to predict the possible metabolic fate of drugs and carcinogens in the body.

However, these models require to be verified experimentally by some indirect techniques, including e.g. spectroscopic methods, site-directed mutagenesis studies, and protein modification techniques using mechanism-based inhibitors, affinity or photoaffinity probes to determine critical amino acids involved in substrate binding (Domanski and Halpert 2001; Kent et al. 2001; Gartner 2003). Though the approach of the site-directed mutagenesis is frequently used for identification of amino acid residues important for substrate binding/specificity, precautions should be taken when the data are interpreted. One amino acid substitution changing the mutated target may also affect the form taken by other motifs, either near or remote from the change by communication and interactions within the whole protein (Conley et al. 2001).

For validation of our CYP 2B4 model we used a technique of photoaffinity labeling. Photoaffinity labeling, besides the other protein modification techniques, has been successfully applied for labeling of several CYPs, revealing active center amino acids (Ohnishi et al. 1993; Cvrk et al. 1996; Cvrk and Strobel 1998; Gartner 2003). Photoaffinity probes are usually photolabile derivatives of the enzyme substrate. Irradiation of a binary complex, enzyme-photolabile substrate, causes the formation of a reactive intermediate that binds covalently to the enzyme (Bayley 1983). In our experiments (Antonovič et al. 1999), heterobifunctional photoaffinity probes (varying in their lengths) derived from benzphetamine, an amphetamine with pronounced sympathomimetic stimulant activity in the central nervous system were used. This compound is often used as a specific substrate for CYPs of 2B subfamily and, thus, it is suitable for validation of the reliability of constructed CYP 2B4 model. The photoaffinity probes employed contained azido- and amino-groups on the opposite ends of their molecules. These probes were designed to anchor the probe through the amino group to the heme in the active center of CYP and covalently modify accessible amino acid residues by photoactivated azido-group of a defined distance from the heme.

Using these photoaffinity probes, we were able to prove the CYP 2B4 model validity as well as to uncover the route (substrate access channel) by which the substrate enters the enzyme active center. Thus, the presented 3D structure of

CYP 2B4, verified by experimental data, represent closed conformation that seems to be more compatible with substrate binding and turnover than open conformation determined in the CYP 2B4 crystal (Scott et al. 2003).

Materials and Methods

Materials

Coomassie Brilliant Blue R250 was product of Fluka (Switzerland). PB was purchased from Kulich (Czech Republic). Reduced glutathione and silica gel TLC plates were obtained from Merck (Germany). NADPH was purchased from Reanal (Hungary), trifluoroacetic acid (TFA) and somatostatin from Aldrich (Czech Republic). Bicinchoninic acid (BCA) was obtained from Sigma (USA). Diamantane was a generous gift from Pliva-Lachema (Czech Republic). Lys-C (from *Lysobacter enzymogenes*) was a product of Promega (USA). All other chemicals were of reagent grade or of better quality.

CYP 2B4 homology modeling

The 3D structure of rabbit CYP 2B4 was built based on the crystal structures of following CYPs (PDB code): CYP 2C5/3 (1dt6) (Williams et al. 2000a), CYP 51 (1ea1) (Podust et al. 2001), and CYP 102 (1bu7) (Sevrioukova et al. 1999), found by NIH-NCBI Blast Iterative Service using two iteration runs (Altschul et al. 1990). The sequence of CYP 2B4 was obtained from SwissProt database. The sequence alignment was done in two steps by Modeller 6.2 (Sali and Blundell 1993; Fiser et al. 2000) and Clustal X program (Thompson et al. 1997). In the first step, the known structures were spatially aligned by Modeller 6.2 (using malign 3D function) since the crystal structure of CYP 2C5/3 lacks the N-terminal residues and 10 F-G loop residues. The loop residues were added to the CYP 2C5/3 sequence and aligned to the corresponding residues of CYP 51 and CYP 102 (Clustal X, profile alignment). Finally, the CYP 2B4 was aligned from N-terminal residue 45 to the created alignment among CYP 51, CYP 102, and CYP 2C5/3 by Clustal X (command "align sequence to the profile"), then the CYP 2C5/3 F-G loop residues were removed again. This alignment was subsequently used in the program Modeller 6.2 for generating the model structures. The segment in CYP 2B4, corresponding to F-G loop residues 194–204 in CYP2C5/3, was constructed by Modeller 6.2 (Fiser et al. 2000). The resulting structures were corrected manually (e.g. AA clashes) using the SwissProt Viewer 3.7 (Guex and Peitsch 1997).

In each of the built structures, the heme group has been docked using AutoDock (3.05 software) (Morris et al. 1998) and all of them had been subdued to the energy minimization by Charmm 29 program (Brooks et al. 1983). AutoDock parameters were set as follows: grid spacing 0.15 Å, the heme positioned in the grid center, and used maximum (120) of allowed points. The heme iron charge as well as the length of Cys thiolate-Fe bond were computed using Sybyl program and adjusted based on CYP crystal base structures. Solvation parameters for the heme

were default values in AutoDock Addsol program module. Parameters of algorithm were chosen to be 270,000,000 and 250 and 0.2 for the number of generations, population size and mutation rate, respectively.

After 100 steps of the steepest descent, the resulting model structures were checked using the ProCheck software (Laskowski et al. 1993). The structure with the lowest energy and the best ProCheck score has been used for further energy minimization by Charmm 29 (100 steps of the conjugated gradient followed by 100 steps of the steepest descent). Due to the quite large number of resulting structures produced by the Modeller 6.2, no further molecular dynamics computing has been deployed (Sali and Blundell 1993; Fiser et al. 2000). The CYP 2B4 model was finally analyzed by ProCheck. All of the substrate structures were docked into the model. For docking the AutoDock has been employed, using the genetic algorithm method, with 27,000,000 generations and 200 populations, with 20 runs for each substrate (Morris et al. 1998). The conformation having the lowest energy has been chosen as the result.

The model coordinates in PDB file format are available from the authors upon a request.

Synthesis of photoaffinity probes

Aminoazido probes, N-(p-azidobenzyl)-N-methyl-p-aminobenzylamine/HCl (I), N-(p-azidophenethyl)-N-methyl-p-aminobenzylamine/HCl (II), and N-(p-azidophenethyl)-N-methyl-p-aminophenethylamine/HCl (III), were prepared by partial reduction of corresponding diazido-compounds as described previously by Hodek and Strobel (1994). Final yields of probes I, II and III were 16, 35 and 13%, respectively. The synthesized probes were identified by mass spectroscopy (INCOS 50, Finnigan MAT), IR (PE 684), and NMR (Varian UNITY-INOVA 400) spectra.

Isolation of microsomal fractions and pure isoenzymes

All experiments with laboratory animals were approved and carried out in accordance with the institutional guidelines and rules for laboratory animal handling. Liver microsomal fractions of PB-treated rats or rabbits were prepared according to Guengerich (1977). CYP 2B4 was isolated from rabbit PB liver microsomes as described by Haugen and Coon (1976). Supersomes, microsomes isolated from insect cells transfected with baculovirus constructs containing cDNA of human CYP 2B6 and expressing NADPH : CYP reductase, were from Gentest corp. (Woburn, MA).

CYP difference spectra

Interaction of CYP with photoaffinity probes was followed by difference spectroscopy. Difference spectra were recorded on the spectrophotometer Specord M-40 (Carl Zeiss, Jena, Germany). PB-induced Ms and pure CYP 2B4 were diluted with phosphate buffer (0.1 mol/l K/PO_4, pH 7.4, with 20% glycerol) to 3.3 nmol P450/ml and 2 nmol P450/ml, respectively. After recording the base-line, the CYP

in the sample cuvette was perturbated with gradually increasing amounts of photoaffinity probe (2–700 μmol/l) and the same volume of the probe solvent (water) was added to the reference cuvette. The resulting high-low spin shift of heme iron was monitored as difference spectra from 350 to 500 nm (Hodek and Strobel 1994). Spectral dissociation constants (K_s) were determined as described elsewhere using a double reciprocal plot (Schenkman et al. 1967).

CYP preparative photolabeling

All photolyses were carried out in quartz tubes (2 mm i.d.) at room temperature using a photolyzer purchased from Oriel Corp. (Stratford, CT) equipped with 100 W mercury arc lamp as described by Hodek and Strobel (1994). In brief, CYP samples (rabbit CYP 2B4 or human recombinant CYP 2B6 expressed in supersomes) diluted with Tris/HCl (10 mmol/l, pH 7.2) to the final concentration of 4 nmol P450/ml containing 25 μmol/l probe (I or II) were photolyzed for 20 s in the presence or absence of 6 μmol/l diamantane as well as without any probe. Minor protein impurities and photodegradation products prior the analysis of photoaffinity labeled CYP 2B4 on MALDI-TOF apparatus were separated by SDS-electrophoresis (Laemmli 1970) (10 % separating gel) from all samples.

Analysis of labeled CYP

As described elsewhere (Antonovič et al. 1999), the protein band, corresponding to CYP (2B4 or 2B6), was excised from the gel and digested by Lys-C directly in the gel according to Shevchenko et al. (1996). Resulting peptide mixtures were analyzed on MALDI-TOF mass spectrometer BIFLEX (Bruker-Franzen) using α-cyano-4-hydroxycinnamic acid in aqueous 30 % acetonitrile and 0.1 % TFA as a MALDI-TOF matrix. Post source decay (PSD) spectra were recorded and analyzed for the presence of modified amino acid residue.

Analytical methods

Protein concentrations in the microsomal fractions and pure enzyme preparations were determined by the BCA method using bovine serum albumin as a protein standard (Wiechelman et al. 1988). The concentration of CYP was assayed according to method by Omura and Sato (1964) based on the complex of reduced CYP with CO.

Results and Discussion

CYP 2B4 homology model construction

In recent years, homology modeling of 3D CYP structures based on crystal structures of microbial CYPs has become an important tool to study structure-function relationship of mammalian CYPs. The major limitation of this approach, however, is a low sequence homology between microbial and mammalian CYPs (Kirton et al. 2002). The crystal structure of the first solubilized mammalian CYP,

CYP 2C5/3, provides a more reliable template for better CYP models of membrane-bound CYPs, namely those of CYP 2 family (Williams et al. 2000a; Lewis 2002). Since CYPs of CYP 2B subfamily have been identified to play an important role in metabolism of various xenobiotics, including drugs (Ekins and Wrighton 1999), the task of CYP 2B4 model construction has been undertaken. The homology modeling was used despite the fact that, only recently, the crystal structure of CYP 2B4 was released (Scott et al. 2003). The X-ray crystallography data, based on crystallized truncated enzyme, revealed an open conformation (large cleft extended to the heme moiety) that is trapped by homodimer formation. One might speculate that the unusual open conformation is artificial, caused by the method used. Moreover, the published CYP 2B4 structure does not agree with photoaffinity labeling data obtained with the native enzyme in solution and some data of the site-directed mutagenesis (Antonovič et al. 1999; Scott et al. 2003).

Multiple sequence alignment used for the CYP 2B4 model construction is shown in Figure 1 (page 475). To create the template applicable for CYP 2B4 model-building structures of CYP 51, CYP 102, and CYP 2C5/3 were spatially aligned to overcome missing segments of CYP 2C5/3 as well as highly variable regions of microbial CYPs. To achieve correct heme docking, heme and Cys sulfur charges were computed first using Sybyl and CYP crystal base structures (PDB), and then solvation parameters were added by Addsol software. The heme placement found was the final best pose followed from the assessment the binding distance of Cys sulfur and heme iron and their relative orientation and symmetry, as well as from the results of a further energy minimization, showing the final energy minimum. Moreover, the G-factor of the heme surrounding amino acids in our model structure agreed well with that of known P450 structures. The resulting CYP 2B4 model was finally analyzed by ProCheck. As it is clear from Figure 2, there were no significant differences between the model and the known structures used for the modeling. The final overall model energy was as low as −9851.633 kJ/mol.

Location of substrate binding site key residues

Novel insight obtained with the CYP 2B4 model was provided by docking diamantane (see Figure 3, page 478). The diamantane binding mode shown therein was the only one orientation characterized by the highest ranking computed by AutoDock runs. Diamantane, this highly specific CYP 2B substrate, fits well the CYP 2B4 binding cavity. This finding is also documented by experimentally determined K_s from difference binding spectra. Diamantane K_s determined with CYP 2B1 and CYP 2B4 (2 μmol/l and 0.5 μmol/l, respectively) represents the lowest one found for CYP 2B substrates (Hodek et al. 1988).

In our model, in agreement with data for all other CYP 2B models based on various templates (Szklarz et al. 1994; Chang et al. 1997; Dai et al. 1998; Lewis 1998; Wang and Halpert 2002), the substrate binding site is localized on the distal side of the heme where oxygen molecule activation occurs. Analysis of the substrate binding site within the distance of 4 Å from carbon skeleton of diamantane revealed

Table 1. Key active site amino acid residues of CYP 2B4 model structure in contact with diamantane

Amino acid residue	Sequence position in CYP 2B4	Assignment to CYP secondary structure	Experimentally identified by
Ile **	101	helix B′	Dai et al. (1998)
Asp	105	helix B′-C loop	Dai et al. (1998)
Ile *	114	helix B′-C loop	Domanski and Halpert (2001) Wang and Halpert (2002)
Phe	115	helix B′-C loop	Domanski and Halpert (2001)
Phe *	297	helix I	Dai et al. (1998)
Ala	298	helix I	Domanski and Halpert (2001)
Thr *	302	helix I	Domanski and Halpert (2001) Kent et al. (2001)
Ile *	363	K-β1-4 loop	Domanski and Halpert (2001) Wang and Halpert (2002)
Val *	367	K-β1-4 loop	Domanski and Halpert (2001)
Val **	477	βhairpin	Domanski and Halpert (2001)

Presented amino acid residues are within 4 Å distance from diamantane skeleton. * residues are within 3.5 Å, ** residues are within 3.0 Å.

key amino acid residues responsible for the substrate recognition and orientation (see Table 1). CYP substrates are mostly hydrophobic compounds, accordingly, identified amino acid residues, lining the substrate binding pocket, with exception of Thr 302 and Asp 105, are hydrophobic, too. The side chain of Thr 302, close to the heme plane, is known to be involved in the oxygen/binding activation. Similarly in previously published 2B1 model, acidic amino acid residue Asp 105, identified in a middle part of the model substrate binding site, corresponds to homologous Glu 105 predicted in formation of salt bridge with the positively charged benzphetamine nitrogen (Poulos et al. 1987). Several identified binding site residues found in contact with diamantane have been tested by site-directed mutagenesis. Thus, involvement of seven of nine key residues in the CYP 2B4 binding site cavity has been confirmed experimentally (Domanski and Halpert 2001) (Ile 114, Phe 115, Ala 298, Thr 302, Ile 363, Val 367, Val 477). Additional residues, Ile 101 and Phe 297, determined from our CYP 2B4 model, are highly conserved along CYP 2B family and were suggested to play an important role in binding site as shown in CYP 2B1 model structure (Dai et al. 1998).

Moreover, the position of docked substrate in the CYP 2B4 model was assessed from the view point of restrains deduced from results of CYP 2B mediated metabolism of diamantane. In the CYP 2B4 model, diamantane is oriented to expose its backbone C3 and C4 towards the heme plane in a distance of 4.9 and 5.0 Å from the iron, respectively. From the crystallographic structures of CYPs (e.g. CYP 101, CYP 107A1, CYP 2C5/3) in complex with substrates (Poulos et al. 1987;

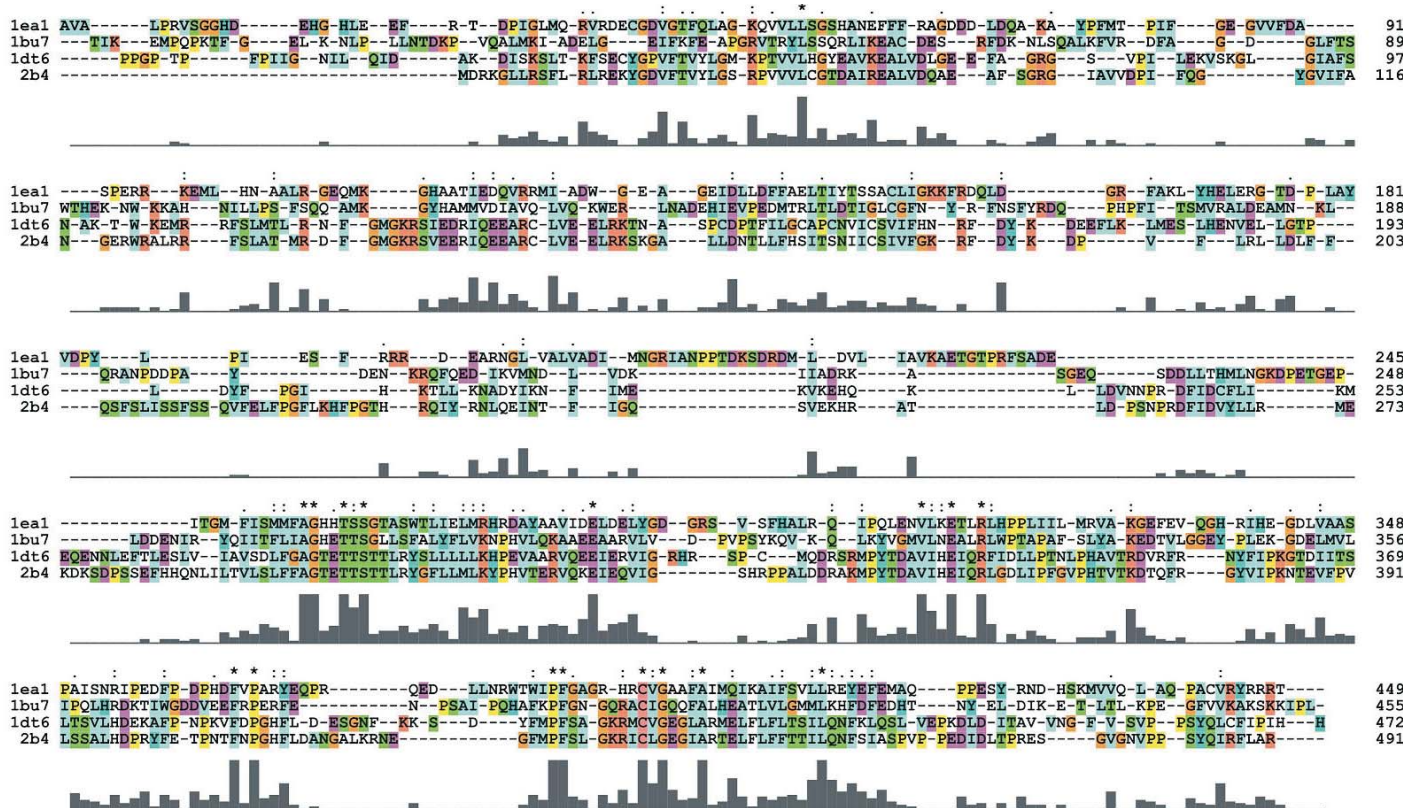

Figure 1. Multiple sequence alignment among crystallized templates and primary structure of CYP 2B4 (P00178 – SwisProt accession number http: www.expasy.ch). Template sequences: 1ea1, 1bu7 and 1dt6 (in PDB code) of CYP 51, CYP 102 and CYP2C5/3, respectively, were obtained from the PDB (http://www.rcsb.org/pdb) and numbered according to their full lengths. Primary structures of CYP 2C5/3 and CYP 2B4 were shortened by 11 and 45 amino acid residues form their N-terminus (membrane domain) to be properly aligned. In addition, CYP 2C5/3 residues 194–204 could not be aligned since it was missing in the CYP 2C5/3 crystal structure. Similarities among the sequences are expressed as a block-plot under the alignment.

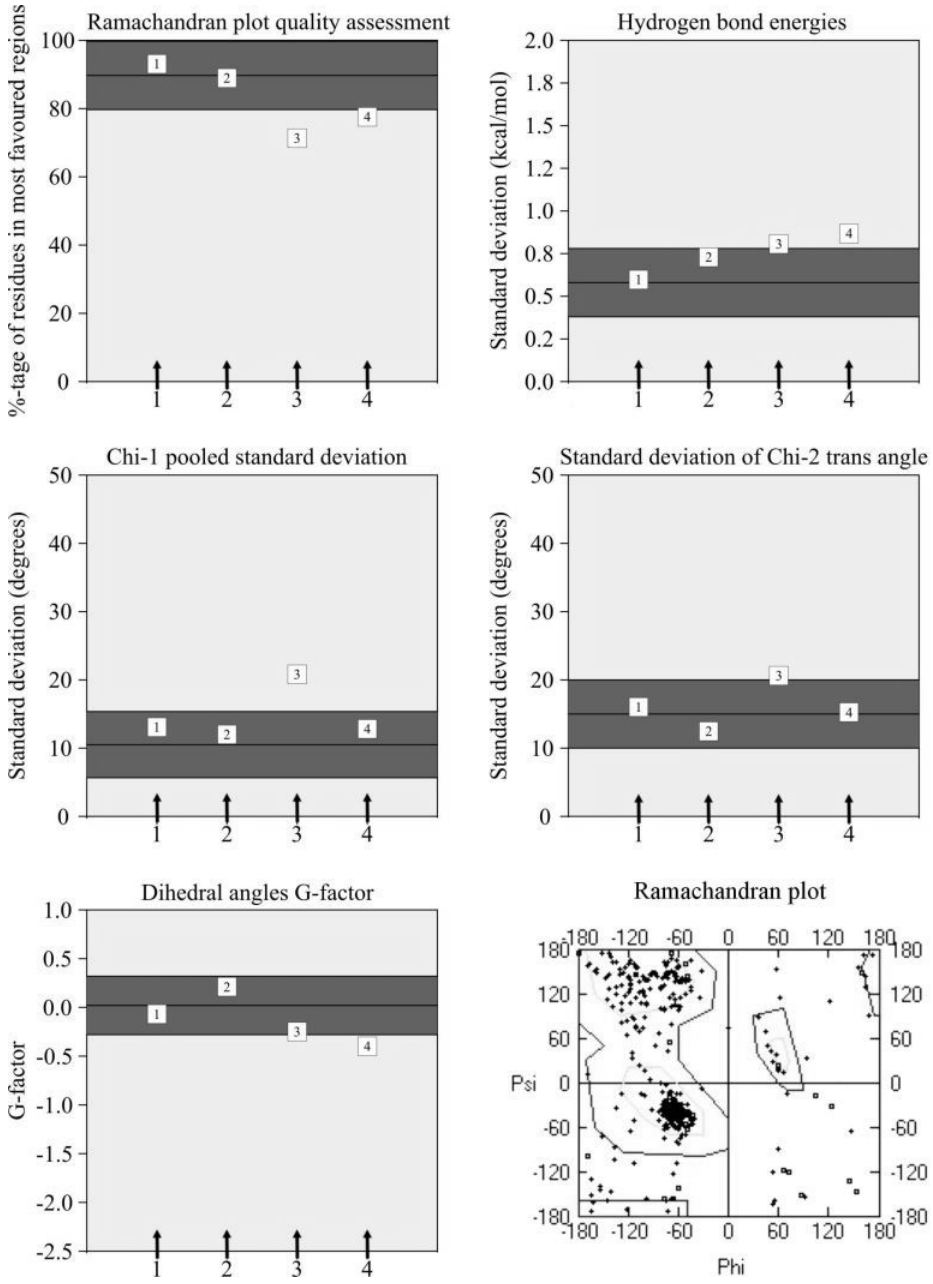

Figure 2. Analysis of structural parameters of CYP 2B4 model (4) in comparison with known structures of CYP 102 (1), CYP 51 (2), and CYP2C5/3 (3). Shaded areas represent intervals in which 95% of protein X-ray structures occur (Laskowski et al. 1993). Bottom right panel shows a Ramachandran plot of the CYP 2B4 model.

Cupp-Vickery and Poulos 1995; Schlichting et al. 2000; Wester et al. 2003), it is clear that the distance between the carbon, at which hydroxylation takes place, and heme iron is 4.5–4.8 Å or even 5.3 Å based on molecular dynamics simulations (Paulsen et al. 1991). A similar distance of 4.8 Å between heme iron and site of hydroxylation was determined when natural substrate, progesterone, was docked to crystal structure of CYP 2C5/3 (Williams et al. 2000b). The substrate hydroxylation is suggested to proceed *via* abstraction of substrate hydrogen atom by the oxy-ferryl intermediate. Therefore, the probability of hydroxylation should be assessed based on H-O distance. Considering the presence of an activated oxygen atom bound to heme iron (ferryl oxygen), hydrogen atom of C4 diamantane position is much closer (2.6 Å) to the reactive oxygen atom than hydrogen atoms of C3 position (3.4 and 3.8 Å). Thus, the steric conditions of docked diamantane imply a better accessibility of diamantane C4 hydrogen for abstraction by oxygen that should result in a preferred formation of 4-hydroxyderivative of diamantane. This prediction of diamantane hydroxylation site agrees well with experimental data. In a reconstituted microsomal system, diamantane is metabolized prevailingly to 4-hydroxyderivative (∼50%) and in a minor extent to C3-derivatives, 3-oxodimantane and 3-hydroxydiamantane, (total ∼10%) (Hodek et al. 1988). Comparison of the observed diamantane orientation relative to heme, as well as the involvement of identified key amino acid residues for its binding with results of metabolic and site-directed studies, respectively, supports the reliability of the central part of the constructed model.

Photoaffinity probe difference spectra

Photoaffinity labeling of CYP offers a unique insight into the structure of native enzymes in solution. This is the major advantage of photoaffinity labeling in contrast to the most respected approach of X-ray crystallography, which is limited to use of mutated and truncated mammalian CYPs that is necessary for their crystallization. In addition to potential CYP structural changes caused by crystallization (e.g. dimerization, presence of ions), effect of prokaryotic CYP expressing system on a proper protein folding has to be considered, too.

To further validate the CYP 2B4 model aminoazido-derivatives of benzphetamine (see Figure 4) have been designed for photoaffinity labeling the CYP 2B binding site and/or access channel within defined distances from the heme (Ohnishi et al. 1993; Hodek and Strobel 1994). These derivatives are expected to be coordinated to the heme iron as its sixth ligand *via* their amino-group, while the opposite end of the molecule (containing the photolabile azido-group) is located in distal regions of the active center cavity. To determine whether the photoaffinity probes do bind the heme iron as their ligand, the difference spectroscopy was employed. This technique allows the direct examination of changes in heme iron coordination (Schenkman et al. 1967). The interaction of the probes with CYP in PB-induced Ms and purified 2B4 was examined by difference spectroscopy in order to select the probe meeting our criteria of anchoring to the heme iron. According to the position of spectral maxima and minima, the probes were classified as either compounds

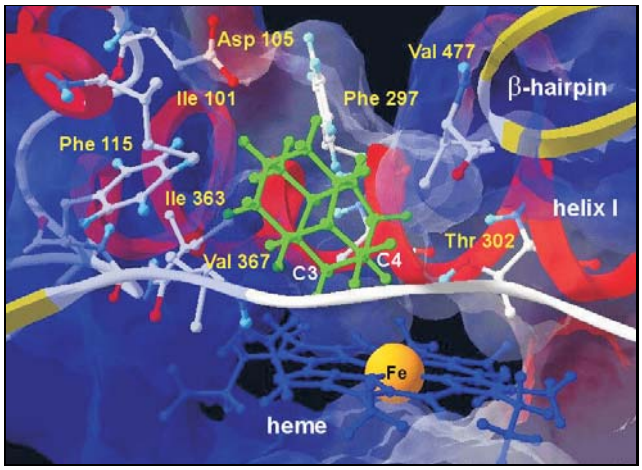

Fig. 3A

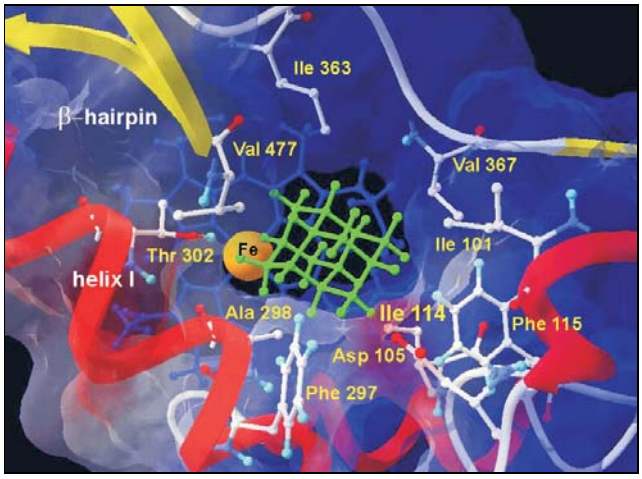

Fig. 3B

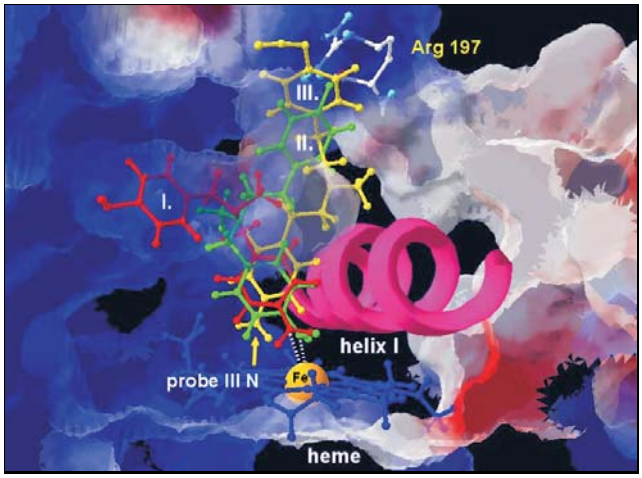

Fig. 5

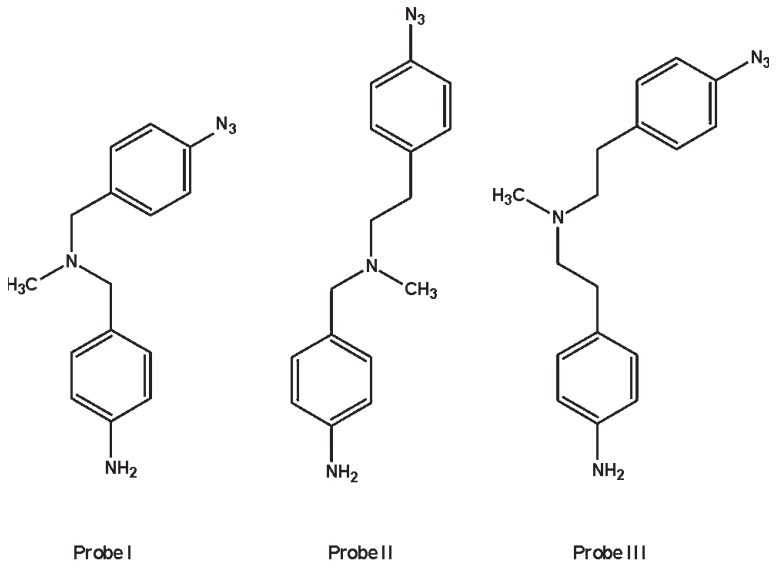

Figure 4. Structures of heterobifunctional photoaffinity probes.

coordinating heme iron, heme ligands, (max. ∼432 nm, broad min. ∼415 nm) or compounds not interacting with the heme iron (max. ∼387 nm and min. ∼418 nm) (Schenkman et al. 1967). Difference spectra of CYP 2B4 with probes I and II revealed a pronounced shift of an absorption maximum to about 432 nm (type II binding spectra) indicating heme coordination by primary amines (see Table 2). Hence, these heme binding ligands were selected as potential photoaffinity probes. On the other hand, probe III was oriented in the active center in a different way not allowing heme coordination – only type I binding spectra were detected. The explanation of this effect might follow from docking experiments discussed below. Moreover, a photoaffinity probe should bind the enzyme active center with high binding affinity to assure specificity of photoaffinity labeling (Bayley 1983). From

Figure 3. Active site of CYP 2B4 model with docked diamantane. Amino acid residues (in CPK) within the distance of 4 Å from diamantane skeleton (in green) are presented. **A.** (side-view) shows diamantane orientation (positions C3 and C4) relative to the heme plane (in blue), **B.** (top-view) amino acid residues lining the substrate binding site.

Figure 5. Photoaffinity probes docked in the CYP 2B4 model. Structure of CYP 2B4 in a close vicinity to heme (in blue) illustrates the active center architecture. Superimposed probes I and II (in red and green, respectively) are pointing their amino group towards the heme iron, while probe III (in yellow) turns it away.

Table 2. Spectroscopic data characterizing CYP interaction with photoaffinity probes

Photoaffinity probe	Type of binding	K_s (μmol/l)		$\Delta A_{max} \cdot 10^3$	
I	Ligand (type II)	1.1	14.6	17.8	33.2
II	Ligand (type II)	9.6	37.2	40.3	57.6
III	Substrate (type I)	6.0	36.2	8.0	27.5

The Table contains two sets of values for each parameter corresponding to the bi-phasic process of probe binding to CYP. K_s, spectral dissociation constant; ΔA_{max}, absorption difference at saturation.

the difference spectra with each photoaffinity probe, K_s were determined, reflecting their strong binding affinity (Table 2).

Photoaffinity labeling of CYP 2B4

Based on the results of difference spectroscopy, probes I and II were employed for photoaffinity labeling of purified CYP 2B4. In addition to labeling CYP 2B4 with the probes alone, CYP 2B4 labeling was also performed in the presence of the probe competitor, diamantane, a specific CYP 2B4 substrate (Hodek et al. 1988), able to displace the probe from the active center (Hodek et al. 1995). The role of diamantane was to prevent probe incorporation into the enzyme active center and thus to allow the assessment of the labeling specificity. Upon UV-irradiation, an azido-group of the probe is photolyzed to nitrogen molecule and reactive nitrene-intermediate. Samples of photoaffinity-labeled CYP 2B4 were digested by proteinase Lys-C, and the mixture of resulting CYP 2B4 peptides was analyzed on a MALDI-TOF apparatus. Using this technique, masses of the individual peptides were determined in each sample. When comparing data of MALDI-TOF mass spectra for probe I in presence and absence of competitor, it is evident that no specific labeling occurred (data not shown). On the other hand, as we have published previously (Antonovič et al. 1999), probe II specifically labeled CYP 2B4. The labeled hexapeptide DPVFLR from the position 192–197 of a CYP 2B4 primary structure occurs only in the sample irradiated in the absence of diamantane. In other words, this peptide-probe adduct is suggested to originate from the enzyme active center. PSD analysis of the adduct indicated Arg 197 to be involved in the adduct formation (Antonovič et al. 1999). Taking into account the length of the expanded probe II (about 14.5 Å) (Cvrk et al. 1996) and the distance between the heme iron atom and nitrogen atom of the probe amino-group (about 2 Å) (Poulos and Howard 1987), the target of probe II labeling, Arg 197, should be located within the maximal distance of 16.5 Å from the heme. The labeled region most likely belongs to the distal structure of the active center or the substrate access channel.

It is worth mentioning that in the case of partly homologous human CYP 2B6, Lys 197 corresponding to Arg 197 of CYP 2B4 was not labeled though nitrene

intermediates nevertheless are able to modify both amino acid residues (Bayley 1983). Thus, the reason for this result is not clear.

Model evaluation by photoaffinity probe docking

All three photoaffinity probes were docked to the model active center (see Figure 5, page 478) to explain the manner of probe interactions found by difference spectroscopy. This approach allowed us to assess also the position of the target amino acid labeled by probe II within the model structure. As a prerequisite for the probe I–III docking, the formation of heme iron complex was set as one of the rules to exclude unsuitable AutoDock results. Beside the energy ranking, water cluster introduction into the CYP 2B4 binding site was used as an additional criterion to evaluate the possibility of the complex formation. The application of both approaches revealed the best poses of probe-bound CYP 2B4 indicating that probes I and II can readily bind *via* their amino-group ligations to heme iron, since the distances between probe I and II amino-group nitrogens and heme iron are 3.0 and 2.5 Å, respectively. These values are within normal limits of Fe-N distances in crystallized complexes of CYPs with inhibitors (Poulos and Howard 1987; Raag et al. 1993). On the other hand, although probe III is bound facing the heme with amino-group, the Fe-N distance of 3.9 Å does not allow an effective heme iron ligation. This observation is consistent with the spectral shift of Soret absorption maximum found in difference spectra (Table 2). While probes I and II caused formation of type II spectra, as heme ligands (typical maximum > 420 nm), probe III induced type I spectra (Schenkman et al. 1967) proving the absence of heme iron binding. The structural base of these differences were further examined using the CYP 2B4 model. Similarly to benzphetamine, all probes contain positively charged nitrogen in their molecule, however, its distance from the terminal amino-group, being the same for probe I and II, is by one methylene group longer for probe III (Figure 4). This difference in position of the positively charged center most likely affects the probe interactions in the binding site. The structure of binding pocket was examined within 5 Å radius from the probe III positively charged N for negatively charged amino acid residues, the potential counterpart for the salt bridge, which might be a driving force determining probe III binding orientation. Only the negatively charged residue Glu 256, found in the distal region (about 12 Å from heme), is likely to be engaged in a salt bridge formation. The distance of about 4 Å between probe III nitrogen and carboxyl-oxygen atom is optimal for formation of this type of salt bridge. In the case of probes I and II, even the shortest distances between Glu 256 carboxyl-oxygen atom and the probe positively charged centers 7.4 and 6.3 Å, respectively, are not suitable for an efficient ion pairing. Hence, the suggested probe III stabilization in a positioned with the amino-group away from the heme iron is responsible for observed lack of heme ligation. Moreover, another acidic residue, Asp 105, found in a close vicinity (4.3 Å) of positively charged nitrogen in probes I and II, most probably helps to maintain the proper probe orientation.

Further support for our model can be deduced from the fact that CYP 2B4 was labelled only by probe II. Examining the CYP 2B4 model structure with docked

probes, no target for modification (like Lys or Arg side chains) in a proper distance from the probe I nitrene was found. On the other hand, heme-anchored probe II in the CYP 2B4 model points its reactive nitrene towards side chain of Arg 197. The distance of 2.2 Å between C-guanidyl moiety and N-nitrene made the labeling of Arg 197 feasible. Since probe II upon binding passes through the substrate access channel, we were able to determine the distance between surface amino acid residues and the heme. This approach thus confirmed the reliability of the model and identified distal regions of the substrate access channel. Unfortunately, a direct comparison with already published CYP homology models is rather limited since the available data are focused mainly on amino acid residues of the lower part of the active site, and no coordinates of 3D models have yet been released.

On the other hand, in the 3D structure of CYP 2B4 (PDB code 1po5), based on the crystal (Scott et al. 2003), the identified Arg 197 amino acid residue is located in a distance from the heme iron that is out of the probe II labeling range. The closest guanidyl nitrogen atom of the labeled Arg is 25.5 Å away from the heme. Thus, the open conformation determined in CYP 2B4 crystal is not consistent with our data. The comparison of both, crystal and model CYP 2B4 structures, is shown in Figure 6.

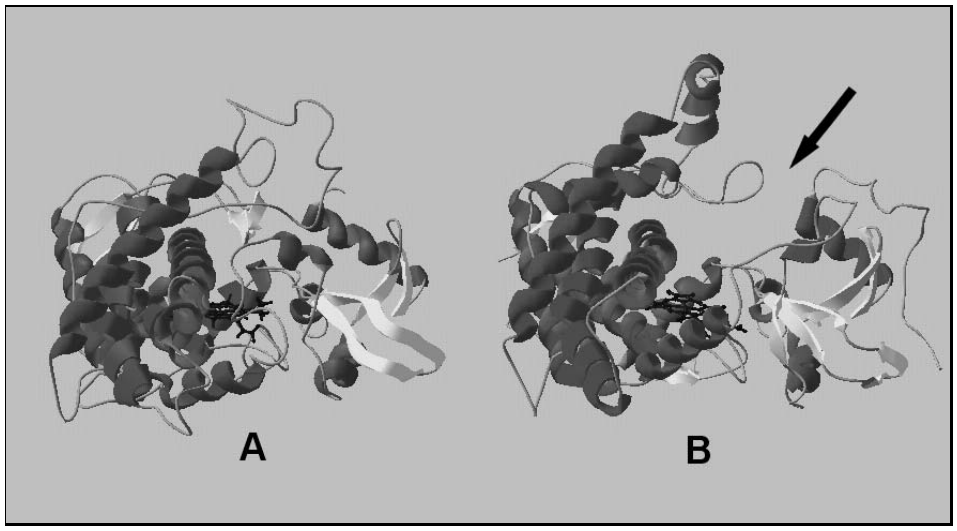

Figure 6. Comparison of CYP 2B4 structures. **A.** The model structure represents a closed CYP 2B4 conformation. **B.** The crystal structure (PDB code 1po5) in open conformation shows a wide cleft extended to the heme.

Location of CYP 2B4 substrate access channel

The buried CYP active center implies the presence of a channel connecting the protein exterior and the binding site. Using homology modeling, the opening to

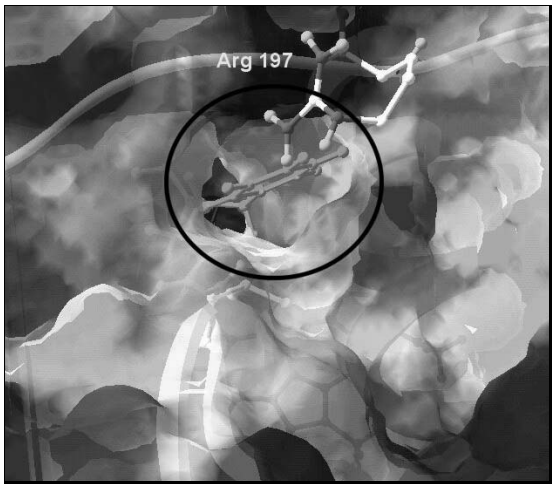

A

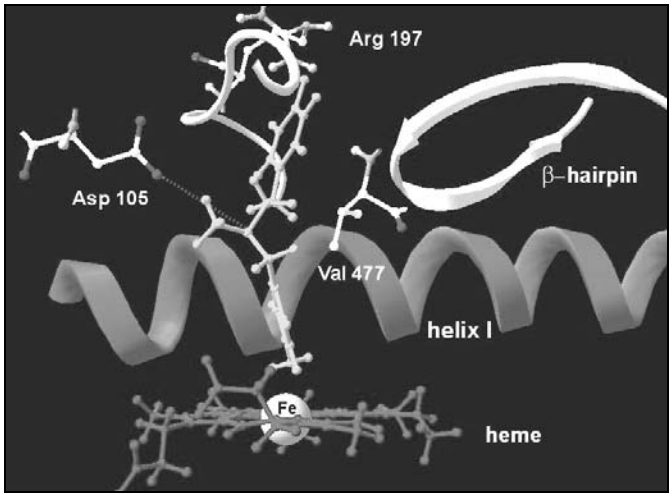

B

Figure 7. View of substrate access channel. In panel **A**, top-view of the access channel entry is shown in circle. Upper hydrophobic chain contains the labeled Arg 197 residue. Val 477 residue is located in the turn of β-hairpin structure. Panel **B** presents a side-view of probe II anchored to heme. Asp 105 is engaged in the salt bridge formation with the probe II nitrogen.

the substrate access channel of mammalian CYPs was predicted to different surface regions – below helix F in the proximity of helix E, possibly at the end of helix F behind F-G loop, or between F-G loop and N-terminal β-sheet (Szklarz et al. 1994; Chang et al. 1997; Peterson and Graham 1998). Even the crystal structures of mammalian solubilized CYP 2C5/3 did not solve the issue of the access channel entry with certainty. There is a speculation on two possible routes of substrate

access: the first, similarly to bacterial CYP 102, between F-G loop and N-terminal β-sheet and the second through loose packing of the B-C loop with helices G and I (Williams et al. 2000a). Our present data provide the first experimental evidence for the topology of substrate access channel of mammalian membrane-bound CYPs. Photoaffinity probe II, interconnecting heme with the protein surface, highlighted the gate and route by which CYP 2B4 substrate enters and approaches the buried active center (see Figure 7). The access channel opening is a cleft below the highly hydrophobic chain (containing Phe 195, Leu 196, Arg 197, Leu 198, Leu 199), proceeding on the surface almost perpendicularly to inert helix I. From the side, the channel opening is limited by Val 477 residue, located in the turn of β-hairpin (antiparallel β-sheets 474–480). Most probably hydrophobic residues forming the "mouth" of the access channel participate in substrate recognition that involves its initial docking and determines a proper substrate orientation. The lower part of the access channel is constituted of already identified binding site residues (e.g. Ile 101, Phe 297, Val 477) which are in a close proximity to probe II. Assignment of the identified Arg 197 to any particular structural region within the common CYP protein fold is rather ambiguous because of the low homology in the E-F-G helix region among microbial CYPs themselves, and the much lower homology between mammalian and microbial CYP sequences. Thus, the position of the labeled peptide is suggested to span to the end of E-F loop, or to F helix N-terminus, depending on the alignment used. An exclusion of F-G loop region from the access channel structure of CYP 2B family follows also from data of site-directed mutagenesis data. Mutation analysis of this region in CYP 2B1 suggests that the substrate access may occur via a route that does not involve residues of the F-G loop region (Scott et al. 2002).

Conclusions

The structural model of CYP 2B4 has been constructed based on the CYP 2C5/3 template using homology modeling without any restrains concerning a binding site region and a distal CYP 2B4 structure. Assessment of binding site key amino acid residues and distances across the CYP 2B4 model structure using, metabolic, site-directed and photoaffinity labeling studies demonstrated the reliability of the constructed model without any need of revisions or structure refinements. Modeling and experimental results demonstrated not only the architecture of the substrate binding site, but also indicated the structure of the substrate access channel. It is likely that the constructed CYP 2B4 model represents a closed conformation of the enzyme in the presence of the substrate, in contrast to the substrate-free open enzyme conformation determined in the CYP 2B4 crystal. This possible high structural flexibility may help in understanding CYP 2B4 function and mechanism, and provide some foundation for the rational design of drugs and inhibitors.

Acknowledgements. The work was supported by grant MSM-113100001 from the Czech

Ministry of Education. We thank Pliva-Lachema for kindly providing diamantane sample and Dr. Martinek for optimizing probe structures. The authors are grateful to S. Ekins (Lilly Res. Labs, IN, USA) for provision of the recombinant CYP 2B6.

References

Altschul S. F., Gish W., Miller W., Myers E. W., Lipman D. J. (1990): Basic local alignment search tool. J. Mol. Biol. **215**, 403—410

Antonovič L., Hodek P., Smrček S., Novák P., Šulc M., Strobel H. W. (1999): Heterobifunctional photoaffinity probes for cytochrome P450 2B. Arch. Biochem. Biophys. **370**, 208—215

Bayley H. (1983): Photogenerated reagents in biochemistry. In: Laboratory Techniques in Biochemistry and Molecular Biology (Eds. T. S. Work and R. H. Burdon), pp. 168—180, (2nd ed.), Elsevier Science, Amsterdam

Brooks B. R., Bruccoleri R. E., Olafson B. D., States D. J., Swaminathan S., Karplus M. (1983): CHARMM: A program for macromolecular energy, minimization, and dynamics calculations. J. Comput. Chem. **4**, 187—217

Chang Y.-T., Stiffelman O. B., Vakser I. A., Loew G. H., Bridges A., Waskell L. (1997): Construction of a 3D model of cytochrome P450 2B4. Protein Eng. **10**, 119—129

Conley A., Mapes S., Corbin C. J., Greger D., Walters K., Trant J., Graham S. (2001): A comparative approach to structure-function studies of mammalian aromatases. J. Steroid. Biochem. Mol. Biol. **79**, 289—297

Cupp-Vickery J. R., Poulos T. L. (1995): Structure of cytochrome P450eryF involved in erythromycin biosynthesis. Nat. Struct. Biol. **2**, 144—153

Cvrk T., Strobel H. W. (1998): Photoaffinity labeling of cytochrome P4501A1 with azidocumene: identification of cumene hydroperoxide binding region. Arch. Biochem. Biophys. **349**, 95—104

Cvrk T., Hodek P., Strobel H. W. (1996): Identification and characterization of cytochrome P4501A1 amino acid residues interacting with a radiolabeled photoaffinity diazido-benzphetamine analogue. Arch. Biochem. Biophys. **330**, 142—152

Dai R., Pincus M. R., Friedman F. K. (1998): Molecular modeling of cytochrome P450 2B1: mode of membrane insertion and substrate specificity. J. Protein Chem. **17**, 121—129

Domanski T. L., Halpert J. R. (2001): Analysis of mammalian cytochrome P450 structure and function by site-directed mutagenesis. Curr. Drug Metab. **2**, 117—137 (and references therein)

Ekins S., Wrighton S. A. (1999): The role of CYP2B6 in human xenobiotic metabolism. Drug Metab. Rev. **31**, 719—754

Ekins S., De Groot M. J., Jones J. P. (2001): Pharmacophore and three-dimensional quantitative structure activity relationship methods for modeling cytochrome P450 active sites. Drug Metab. Dispos. **29**, 936—944

Fiser A., Do R. K., Sali A. (2000): Modeling of loops in protein structures. Protein Sci. **9**, 1753—1773

Gartner C. A. (2003): Photoaffinity ligands in the study of cytochrome P450 active site structure. Curr. Med. Chem. **10**, 671—689

Guengerich F. P. (1977): Separation and purification of multiple forms of microsomal cytochrome P-450. Activities of different forms of cytochrome P-450 towards several compounds of environmental interest. J. Biol. Chem. **252**, 3970—3979

Guex N., Peitsch M. C. (1997): SWISS-MODEL and the Swiss-PdbViewer: an environment for comparative protein modeling. Electrophoresis **18**, 2714—2723

Hasemann C. A., Ravichandran K. G., Peterson J. A., Deisenhofer J. (1994): Crystal structure and refinement of cytochrome P450terp at 2.3 Å resolution. J. Mol. Biol. **236**, 1169—1185

Haugen D. A., Coon M. J. (1976): Properties of electrophoretically homogeneous phenobarbital-inducible and beta-naphthoflavone-inducible forms of liver microsomal cytochrome P-450. J. Biol. Chem. **251**, 7929—7939

Hodek P., Strobel H. W. (1994): Synthesis and characterization of azidobenzphetamine analogs of the cytochrome-P450 substrate benzphetamine. Bioorg. Chem. **22**, 253—267

Hodek P., Janščák P., Anzenbacher P., Burkhard J., Janků J., Vodička L. (1988): Metabolism of diamantane by rat liver microsomal cytochromes P-450. Xenobiotica **18**, 1109—1118

Hodek P., Burkhard J., Janků J. (1995): Probing the cytochrome P-450 2B1 active site with diamantoid compounds. Gen. Physiol. Biophys. **14**, 225—239

Ito S., Matsuoka T., Watanabe I., Kagasaki T., Serizawa N., Hata T. (1999): Crystallization and preliminary X-ray diffraction analysis of cytochrome P450sca-2 from Streptomyces carbophilus involved in production of pravastatin sodium, a tissue-selective inhibitor of HMG-CoA reductase. Acta Crystallogr., D. Biol. Crystallogr. **55**, 1209—1211

Kent U. M., Juschyshyn M. I., Hollenberg P. F. (2001): Mechanism-based inactivators as probes of cytochrome P450 structure and function. Curr. Drug Metab. **2**, 215—243

Kirton S. B., Baxter C. A., Sutcliffe M. J. (2002): Comparative modelling of cytochromes P450. Adv. Drug Deliv. Rev. **54**, 385—406

Laemmli U. K. (1970): Cleavage of structural proteins during the assembly of the head of bacteriophage T4. Nature **227**, 680—685

Laskowski R. A., MacArthur M. W., Moss D. S., Thornton J. M. (1993): PROCHECK – a program to check the stereochemical quality of protein structures. J. Appl. Cryst. **26**, 283—291

Lewis D. F. (1998): The CYP2 family: models, mutants and interactions. Xenobiotica **28**, 617—661

Lewis D. F. (2002): Homology modelling of human CYP2 family enzymes based on the CYP2C5 crystal structure. Xenobiotica **32**, 305—323

Leys D., Mowat C. G., McLean K. J., Richmond A., Chapman S. K., Walkinshaw M. D., Munro A. W. (2003): Atomic structure of Mycobacterium tuberculosis CYP121 to 1.06 Å reveals novel features of cytochrome P450. J. Biol. Chem. **278**, 5141—5147

Morris G. M., Goodsell D. S., Halliday R. S., Huey R., Hart W. E., Belew R. K., Olson A. J. (1998): Automated docking using a Lamarckian genetic algorithm and an empirical binding free energy function. J. Comp. Chem. **19**, 1639—1662

Nelson D. R., Strobel H. W. (1988): On the membrane topology of vertebrate cytochrome P-450 proteins. J. Biol. Chem. **263**, 6038—6050

Ohnishi T., Miura S., Ichikawa Y. (1993): Photoaffinity labeling of cytochrome P-45011 beta with methyltrienolone as a probe for the substrate binding region. Biochim. Biophys. Acta **1161**, 257—264

Omura T., Sato R. (1964): The carbon monoxide-binding pigment of liver microsomes. I. Evidence for its hemoprotein nature. J. Biol. Chem. **239**, 2370—2378

Park S. Y., Shimizu H., Adachi S., Nakagawa A., Tanaka I., Nakahara K., Shoun H., Obayashi E., Nakamura H., Iizuka. T., Shiro Y. (1997): Crystal structure of nitric oxide reductase from denitrifying fungus Fusarium oxysporum. Nat. Struct. Biol. **4**, 827—832

Paulsen M. D., Bass M. B., Ornstein R. L. (1991): Analysis of active site motions from a 175 picosecond molecular dynamics simulation of camphor-bound cytochrome

P450cam. J. Biomol. Struct. Dyn. **9**, 187—203
Peterson J. A., Graham S. E. (1998): A close family resemblance: the importance of structure in understanding cytochromes P450. Structure **6**, 1079—1085
Podust L. M., Poulos T. L., Waterman M. R. (2001): Crystal structure of cytochrome P450 14alpha-sterol demethylase (CYP51) from Mycobacterium tuberculosis in complex with azole inhibitors. Proc. Natl. Acad. Sci. U.S.A. **98**, 3068—3073
Podust L. M., Kim Y., Arase M., Neely B. A., Beck B. J., Bach H., Sherman D. H., Lamb D. C., Kelly S. L., Waterman M. R. (2003): The 1.92-Å structure of Streptomyces coelicolor A3(2) CYP154C1. A new monooxygenase that functionalizes macrolide ring systems. J. Biol. Chem. **278**, 12214—12221
Porter T. D., Coon M. J. (1991): Cytochrome P-450. Multiplicity of isoforms, substrates, and catalytic and regulatory mechanisms. J. Biol. Chem. **266**, 13469—13472
Poulos T. L., Howard A. J. (1987): Crystal structures of metyrapone- and phenylimidazole-inhibited complexes of cytochrome P-450cam. Biochemistry **26**, 8165—8174
Poulos T. L., Finzel B. C., Gunsalus I. C., Wagner G. C., Kraut J. (1985): The 2.6-Å crystal structure of Pseudomonas putida cytochrome P-450. J. Biol. Chem. **260**, 16122—16130
Poulos T. L., Finzel B. C., Howard A. J. (1987): High-resolution crystal structure of cytochrome P450cam. J. Mol. Biol. **195**, 687—700
Raag R., Li H., Jones B. C., Poulos T. L. (1993): Inhibitor-induced conformational change in cytochrome P-450CAM. Biochemistry **32**, 4571—4578
Ravichandran K. G., Boddupalli S. S., Hasermann C. A., Peterson J. A., Deisenhofer J. (1993): Crystal structure of hemoprotein domain of P450BM-3, a prototype for microsomal P450's. Science **261**, 731—736
Sali A., Blundell T. L. (1993): Comparative protein modelling by satisfaction of spatial restraints. J. Mol. Biol. **234**, 779—815
Schenkman J. B., Remmer H., Estabrook R. W. (1967): Spectral studies of drug interaction with hepatic microsomal cytochrome. Mol. Pharmacol. **3**, 113—123
Schlichting I., Berendzen J., Chu K., Stock A. M., Maves S. A., Benson D. E., Sweet R. M., Ringe D., Petsko G. A., Sligar S. G. (2000): The catalytic pathway of cytochrome p450cam at atomic resolution. Science **287**, 1615—1622
Scott E. E., He Y. Q., Halpert J. R. (2002): Substrate routes to the buried active site may vary among cytochromes P450: mutagenesis of the F-G region in P450 2B1. Chem. Res. Toxicol. **15**, 1407—1413
Scott E. E., He Y. Q., Wester M. R., White M. A., Chin C. C., Halpert J. R., Johnson E. F., Stout C. D. (2003): A open conformation of mammalian cytochrome P450 2B4 at 1.6-Å resolution. Proc. Natl. Acad. Sci. U.S.A. **100**, 13196—13201
Sevrioukova I. F., Li H., Zhang H., Peterson J. A., Poulos T. L. (1999): Structure of a cytochrome P450-redox partner electron-transfer complex. Proc. Natl. Acad. Sci. U.S.A. **96**, 1863—1868
Shevchenko A., Wilm M., Vorm O., Mann M. (1996): Mass spectrometric sequencing of proteins silver-stained polyacrylamide gels. Anal. Chem. **68**, 850—858
Szklarz G. D., Ornstein R. L., Halpert J. R. (1994): Application of 3-dimensional homology modeling of cytochrome P450 2B1 for interpretation of site-directed mutagenesis results. J. Biomol. Struct. Dyn. **12**, 61—78
Thompson J. D., Gibson T. J., Plewniak F., Jeanmougin F., Higgins D. G. (1997): The CLUSTAL X windows interface: flexible strategies for multiple sequence alignment aided by quality analysis tools. Nucleic Acids Res. **25**, 4876—4882
Wang Q., Halpert J. R. (2002): Combined three-dimensional quantitative structure-activity relationship analysis of cytochrome P450 2B6 substrates and protein homology modeling. Drug Metab. Dispos. **30**, 86—95

Wester M. R., Johnson E. F., Marques-Soares C., Dijols S., Dansette P. M., Mansuy D., Stout C. D. (2003): Structure of mammalian cytochrome P450 2C5 complexed with diclofenac at 2.1 Å resolution: evidence for an induced fit model of substrate binding. Biochemistry **42**, 9335—9345

Wiechelman K. J., Braun R. D., Fitzpatrick J. D. (1988): Investigation of the bicinchoninic acid protein assay: identification of the groups responsible for color formation. Anal. Biochem. **175**, 231—237

Williams P. A., Cosme J., Sridhar V., Johnson E. F., McRee D. E. (2000a): Mammalian microsomal cytochrome P450 monooxygenase: structural adaptations for membrane binding and functional diversity. Mol. Cell **5**, 121—131

Williams P. A., Cosme J., Sridhar V., Johnson E. F., McRee D. E. (2000b): Microsomal cytochrome P450 2C5: comparison to microbial P450s and unique features. J. Inorg. Biochem. **81**, 183—190

Williams P. A., Cosme J., Ward A., Angove H. C., Vinkovic D. M., Jhoti H. (2003): Crystal structure of human cytochrome P450 2C9 with bound warfarin. Nature **424**, 464—468

Yano J. K., Koo L. S., Schuller D. J., Li H., Ortiz de Montellano P. R., Poulos T. L. (2000): Crystal structure of a thermophilic cytochrome P450 from the archaeon Sulfolobus solfataricus. J. Biol. Chem. **275**, 31086—31092

Zerbe K., Pylypenko O., Vitali F., Zhang W., Rouset S., Heck M., Vrijbloed J. W., Bischoff D., Bister B., Sussmuth R. D., Pelzer S., Wohlleben W., Robinson J. A., Schlichting I. (2002): Crystal structure of OxyB, a cytochrome P450 implicated in an oxidative phenol coupling reaction during vancomycin biosynthesis. J. Biol. Chem. **277**, 47476—47485

Final version accepted: September 9, 2004